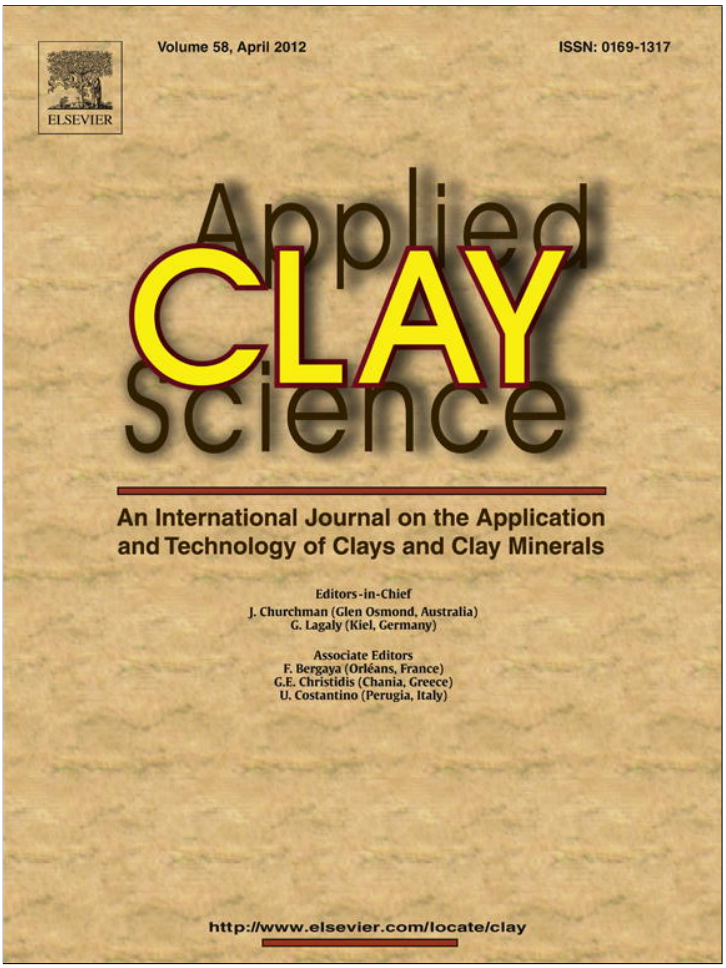

Applied Clay Science 58 (2012) 88–95

Contents lists available at SciVerse ScienceDirect

Applied Clay Science

journal homepage: www.elsevier.com/locate/clay

Research paper

Release of metals from synthetic Cr-goethites under acidic and reductive conditions: Effect of aging and composition

Ana E. Tufo [a], Elsa E. Sileo [a,*], Pedro J. Morando [b,c,d]

[a] INQUIMAE, Departamento de Química Inorgánica, Analítica y Química Física, Facultad de Ciencias Exactas y Naturales, Universidad de Buenos Aires, Pabellón II, Ciudad Universitaria, C1428EHA, Buenos Aires, Argentina
[b] Unidad de Actividad Química, Centro Atómico Constituyentes, Comisión Nacional de Energía Atómica, Avenida General Paz 1499, 1650 San Martín, Provincia de Buenos Aires, Argentina
[c] Instituto de Tecnología J. Sábato, Universidad Nacional de San Martín, Avenida Gral. Paz 1499, 1650 San Martín, Provincia de Buenos Aires, Argentina
[d] Consejo Nacional de Investigaciones Científicas y Técnicas (CONICET), Avenida Rivadavia 1917, C1033AAJ, Buenos Aires, Argentina

ARTICLE INFO

Article history:
Received 10 February 2011
Received in revised form 24 January 2012
Accepted 25 January 2012
Available online 22 February 2012

Keywords:
Cr-goethite
Reductive dissolution
Acid dissolution
Crystallite size
Lattice parameters

ABSTRACT

The dissolution mechanism of pure and Cr-substituted, synthetic goethites with different aging times, as well as the changes in morphology, crystallinity and structural changes, were investigated. The Cr-goethites were obtained by synthesizing goethite in solutions that contained different concentrations of Cr(III) ions. The obtained suspensions were aged in the parent solutions for different time spans. Two samples of pure goethites, prepared using different KOH concentrations, were also studied for comparative purposes.

Chemical analyses showed that Cr-for-Fe substitution was greatest in samples aged for longer time. Rietveld simulation of XRD powder data indicated that the unit cell parameters of pure goethite increased for samples prepared at a higher KOH concentration, and decreased with Cr-incorporation. Simulation also showed that the mean coherence path dimension (MCP), or crystallite size, in the direction perpendicular to crystal plane (110), did not change much in the samples, whereas the crystallite size in the direction parallel to crystal plane (110) increased with Cr-content, KOH concentration and aging time. The obtained MCP values indicate an increasing elongated form in the domains.

Chromium substituted goethites presented a good capacity for immobilizating Cr when the dissolution rates were studied in 3.98 M HCl, 0.10 M oxalic acid (H_2Oxal), and reductive media ($H_2Oxal/Fe(II)$). The shape of the f vs. t profile, where f stands for the fraction of Fe dissolved (dissolved Fe mass/total Fe mass) and t refers to the dissolution time, follows a contracting bidimensional model, and when dissolved in similar acid concentrations, the reactivity follows the trend $HCl < H_2Oxal \ll H_2Oxal/Fe(II)$, indicating that dissolution is noticeably increased in complexing-reducing media. The dissolution rate constant k values were highly depend on crystallite size, and the dissolution rate decreased in the samples aged longest and in goethites containing higher concentrations of Cr. The release of Fe and Cr is congruent and shows a homogeneous distribution of Fe and Cr in the samples. The calculated activation energies values support a surface reaction control for the dissolution process.

1. Introduction

Natural oxides that grow in the presence of different metal cations, may incorporate different elements into its structural framework. Because of this, goethite (α-FeOOH), the most widespread iron hydroxide, is rarely pure and usually contains foreign elements (Carvalho-e-Silva et al., 2003; Lewis and Schwertmann, 1979; Manceau et al., 1999; Norrish, 1975; Schwertmann and Taylor, 1989). The incorporation is the result of the sorption exerted by the highly hydroxylated surface of ferrihydrite over the foreign species to form a mixed ferrihydrite, that acts as a precursor to the more stable oxide goethite (Cornell and Schwertmann, 1996). The incorporation affects the physicochemical properties of goethite such as the unit cell size, structural OH content, thermal and magnetic properties, and dissolution behavior (Gasser et al., 1999; Murad and Schwertmann, 1983; Schwertmann, 1984).

Most research on incorporated goethite has been directed to the substitution of Al(III) for Fe(III) in synthetic samples, as this is the most common substitution in soils (Lim-Nunez and Gilkes, 1987; Ruan and Gilkes, 1995). However, a number of other elements have also been incorporated in synthetic goethite; among them is Cr(III), that forms bracewellite, α-CrOOH, a natural oxide hydroxide isostructural to goethite (Kohler et al., 1997). Metal-for-Fe substitution has been reported for Cr(III) (Schwertmann et al., 1989; Sileo et al., 2004; Singh et al., 2002), manganese (Alvarez et al., 2006; Gasser et al., 1999; Sileo et al., 2001; Stiers and Schwertmann, 1985; Wells et

* Corresponding author. Tel.: +54 11 4576 3380x113; fax: +54 11 4576 3341.
E-mail address: sileo@qi.fcen.uba.ar (E.E. Sileo).

0169-1317/$ – see front matter © 2012 Elsevier B.V. All rights reserved.
doi:10.1016/j.clay.2012.01.018

al., 2006), manganese plus aluminum (Alvarez et al., 2007), cobalt (Alvarez et al., 2008; Pozas et al., 2004), nickel, copper, zinc, cadmium, lead (Gerth, 1990), titanium (Wells et al., 2006), vanadium (Kaur et al., 2009a), and for multi-metal substitution (Kaur et al., 2009b, 2009c, 2010; Singh et al., 2010).

Alteration of bedrocks and especially human activities increase the concentration of toxic metals in soils and aquatic environments. Among others elements, chromium is one of the most toxic anthropogenic metal contaminants that have been introduced to water and soil sediments. Its presence in the environment has resulted from its use in widespread applications such as leather tanning, wood preservation and steel making (Hingston et al., 2001; Khan et al., 2006; Rasem Hasan et al., 2010). Under oxic conditions chromium is present as hydrogen chromate ($HCrO_4^-$) or chromate (CrO_4^{2-}) that may be toxic and carcinogenic at certain concentration levels (U.S. EPA, 1998). Under anoxic conditions, CrO_4^{2-} and $HCrO_4^-$ are readily reduced to Cr(III) by a number of chemicals and microbial species. In particular organic matter has shown to play a significant role in the mobility of chromium in soils because of the tendency of soil organic matter to reduce the mobile Cr(VI) to the relatively immobile Cr(III) (Banks et al., 2006). Chromium (III) is less toxic and less soluble than Cr(VI), and is often sorbed in organic particles, silicate minerals or amorphous Fe(III) (hydr)oxides, even at quite low pH (Baes and Mesmer, 1976). As most sediments are anoxic the reoxidation to Cr(VI) is not easily achieved under the conditions that occur in most natural groundwater environments, and Cr(III)-substituted goethite may be found.

The bioavailability of iron is limited by the low solubility of the Fe(III) oxides. However, the formation of metal–organic surface complexes accelerates hydroxide dissolution (Persson and Axe, 2005; Sparks, 2003), and particularly the presence of Fe(II) or Fe(II)–ligand complexes strongly accelerates the oxide dissolution (Blesa et al., 1987; Borghi et al., 1989; Stone, 1986; Suter et al., 1988; Williams and Scherer, 2004). Although Fe(III) is the predominant state of iron in aqueous and oxygenated environments, the concentration of Fe(II) increases with sediment depth and in the presence of some reducing microorganisms (Cummings et al., 2000; Lovley et al., 2004; Weber et al., 2006).

In the case of Cr-contaminated soils, natural rates of migration of contaminants and soil remediation requires a deep knowledge about the solubility of Cr-incorporated iron oxides. Although it has been established that Cr-goethites present a decreased solubility when compared with pure goethite (Schwertmann et al., 1989; Skovbjerg et al., 2006), the influence of Cr-content, the aging time of goethite in the presence of Cr(III), and the crystallinity of the samples, on the rate and extent of goethite reactivity remains unclear. In this study, we investigate the release of metals in the dark of a series of Cr-substituted goethites that have been obtained from ferrihydrites aged in the presence of Cr(III), at different time spans. Two samples of pure goethites obtained at different pH values, and aged for different times, were also studied. To explore the influence of the media on the release of Fe and Cr, dissolution measurements were performed in non-reductive media at low pH (HCl), in the presence of an organic, surface forming complexes acid (H_2Oxal), and in the presence of Fe(II) and organic acid (H_2Oxal/Fe(II)). The morphology, the structural changes and the crystallinity of all samples were also studied as a function of aging and Cr-content.

2. Materials and methods

2.1. Samples preparations and analysis

Pure and Cr-substituted goethites were prepared following the method of Schwertmann and Cornell (2000), by aging at 70 °C in closed polyethylene flasks, mixtures of 200 mL 3 M KOH and different volumes of 1 M $Fe(NO_3)_3$ and 1 M $Cr(NO_3)_3$ solutions, in the appropriate volume ratio to yield the desired μ_{Cr} ratio (μ_{Cr} [mol%] = [Cr] × 100 / [Cr] + [Fe], [Me] mol L^{-1}). The suspensions obtained were diluted to 2 L, and the total metal content in all preparations was 0.08 M. Four samples containing initial μ_{Cr} values of 0.0; 6.2 ± 0.2, 10.0 ± 0.2 and 37.5 ± 0.2 mol%, were prepared and aged for 20 days (samples named G_0-20, G_5-20, G_7-20 and G_7-20A, where the subscript refers to the actual μ_{Cr} content in the sample). One sample with a nominal μ_{Cr} value of 26.5 was also prepared and aged for 145 days (sample $G_{11.2}$-145).

A second sample of pure goethite was similarly prepared using a 1 M KOH solution and aged for 60 h (G_0–60 h). The products were filtered and in order to remove poorly crystalline compounds two methods were used. Amorphous phases from pure goethites were extracted in the dark with ammonium oxalate (0.20 M, pH 3.0) for 4 h. Amorphous phases in Cr-goethites were dissolved by treatment with 2 M H_2SO_4 solution at 80 °C for 2 h (Schwertmann and Cornell, 2000) because oxalate buffer extraction did not dissolve them completely. The final solids were washed, dialyzed until the conductivity of the solution was similar to that of doubly distilled water, and dried at 50 °C for 48 h. Reagent grade chemicals were used. In all experiments, solutions were prepared with high-purity 18 MΩ cm water.

The total metal content in the goethites was obtained from total dissolution of 70.0 mg of the extracted samples in 6 M HCl, and analysis was made using a GBC, Model B-932 atomic absorption spectrometer

Particle morphology and size were characterized using scanning electron microscopy (SEM) by examining a drop of suspension dried onto a metallic support. A Zeiss Supra 40, field emission, gun-scanning electron microscope was used.

The specific surface area (SSA) of the samples was measured using a Micrometrics AccuSorb 2100 instrument using N_2 as the absorbate (B.E.T. method).

X-ray diffraction (XRD) patterns were obtained using a Siemens D5000 X-ray diffractometer with a Cu target tube and diffracted beam, graphite monochromator. XRD patterns were measured in the 2θ range of 17.5–130°, in 0.025° steps, and 12 s as a counting time. The data were analyzed using the GSAS (Larson and Von Dreele, 1994) system with EXPGUI interface (Toby, 2001).

2.2. X-Ray diffraction refinement

The whole X-ray diffraction pattern was used to refine the crystal structure. Starting unit-cell parameters and atomic coordinates for goethite were taken from the literature (Szytula et al., 1968). Goethite is orthorhombic, space group Pnma (Z = 4). However, it is usually described using the Pbnm group. In order to facilitate comparisons with previous works, the results of our Rietveld simulations are presented in this work using the Pbnm group.

Peak profiles were fitted using the Thompson–Cox–Hastings pseudo-Voigt function (Thompson et al., 1987). As powder diffraction patterns show an anisotropic line-shape broadening that is not a smooth function of *d*-spacing, the mean coherence path dimensions (MCP) or crystallite sizes, were determined in the directions parallel (P_{paral}) and perpendicular (P_{perp}) to the anisotropic broadening (110) axis. Crystallite dimensions were calculated making allowances for the instrument broadening function that was previously modeled using NIST SRM 660 lanthanum hexaboride (LaB_6) standard.

2.3. Acid dissolution experiments

All dissolution measurements were performed in magnetically stirred, thermostated double jacket cells with perforated stoppers provided with pH and temperature sensors, gas inlet and outlet and sampling port. The experiments were conducted in the dark, under a N_2 atmosphere, in 0.50 M $NaClO_4$, at 70.00 ± 0.02 °C. To obtain the

activation energy (Ea) of the dissolution process, kinetic measurements were also performed at 40.00, 50.00 and 60.00 ± 0.02 °C.

Some dissolution behaviors were tested in 0.10 M HCl, but as dissolved Fe was only detected after 46 h, the kinetic runs in mineral acid were conducted using 3.98 M HCl. In a typical experiment the reaction was started by adding the oxide (ca. 20 mg) to 100 mL of 0.10 M H_2Oxal or 3.98 M HCl acid solutions. Approximately 15 aliquots of 1 mL volume each were withdrawn from the suspension during each run, using a micropipette. The aliquots were filtered through a 0.20 μm cellulose acetate membrane.

In experiments designed to probe the influence of ferrous salts, adequate amounts of $Fe(NH_4)_2(SO_4)_2$ (3–35 mg) were added in the dark, and under a N_2 atmosphere, to the 0.10 M H_2Oxal solution. When H_2Oxal acid or H_2Oxal/Fe(II) was used, the pH value was adjusted at 3.50 with sodium hydroxide solutions following previous studies that indicated Fe oxides reach a maximum dissolution rate at this pH value (Baumgartner et al., 1982, 1983). All chemicals were analytical grade and the solutions were prepared with high-purity 18 MΩ cm water.

Dissolved iron concentrations were obtained spectrophotometrically using the thioglycolic acid method (Leussing and Newman, 1956), and chromium was measured by inductively coupled plasma atomic emission spectrometry using a Shimadzu ICPS-1000 III apparatus.

All samples achieved total dissolution in the various dissolving media used and re-precipitation of dissolved metals was not detected. These indicated that the reagent concentrations were sufficient to keep metal ions in the form of soluble complexes.

3. Results and discussion

3.1. Chemical and physical analyses of the solids

Table 1 shows the nominal and the final Cr contents incorporated in the prepared samples. The results and agreement factors of the Rietveld refinements, together with the BET areas, are also shown.

The data show that the maximum uptake of Cr increased with the aging time. Independently, if the sample is prepared from solutions containing μ_{Cr} values of 10.0 ± 0.2 or 37.5 ± 0.2 mol% (samples G_7-20 and G_7A-20), the maximum Cr uptake in goethite aged for 20 days was 7.0 ± 0.2 mol%. Sample $G_{11.2}$-145, prepared from a solution containing μ_{Cr} = 26.5 ± 0.2 mol% and aged for 145 days, shows a molar chromium concentration of 11.2 ± 0.2. The crystallographic characterization and BET areas are discussed latter. Sample G_7A-20 is not included in this work because of the similarity of its metal content when compared to G_7-20.

3.2. Crystal morphology

Fig. 1 shows SEM micrographs for different samples. Particles of pure goethites are elongated; with increasing Cr content, shortening along the length occurs resulting in wider particles.

Pure goethite obtained using 1 M KOH (G_0-60 h) displays the longest particles (1980 × 102 nm) although the aging time is only 60 h (cf. Fig. 1-(a)). In addition, micrographs of sample G_0-60 h clearly show (c.f. micrograph 1-(b) taken at 200,000×) that the acicular particles consist of parallel subunits or intergrowths having a height of approximately 40 nm. Particles of pure goethite aged during 20 days and obtained using 3 M KOH, are shorter and narrower (850 × 85 nm) than G_0-60 h (see Fig. 1-(c)), indicating a larger rate of nucleation. These facts indicate that the growth of the particles is largely determined by the OH^- concentration of the parent iron solution, and the obtained particles become larger at lower OH^- supersaturation.

The width-to-length ratio of the particles is larger in the Cr-goethites (c.f. Table 1) and increases in the more Cr-concentrated particles (see Fig. 1(d) and (e)). The trend is opposite to the one found by Sileo et al. (2001) for Mn-substitution in α-FeOOH that produced acicular crystals. The alteration in morphology has been attributed to preferential adsorption of the additive and, indicates that, in the presence of Cr(III) or Mn(III), growing goethite presents different preferred sites for Fe incorporation, determining a different development of the crystalline faces. In the case of Mn-goethites, Wells et al. (2006) have attributed the morphological changes observed to the structural strain associated with the incorporation of octahedrally distorted Mn(III), that may inhibit lateral development of double chains, resulting a lengthening along the c direction (i.e. length) to produce acicular crystals.

Micrographs of Cr-goethites show evidence of surface etching following the extraction treatment to dissolve amorphous phases. The etching is largest in the more Cr-concentrated sample ($G_{11.2}$-145, see arrows in Fig. 1).

3.3. Rietveld refinement of XRD data and BET areas

The X-ray diffraction patterns showed only goethite as the crystalline phase. The results of the Rietveld simulation are presented in Table 1, together with the cell parameters of bracewellite, α-CrOOH (Milton et al., 1976), isomorphous to goethite. The quality of the

Table 1
Molar chromium content, width-to-length ratio of particles, cell parameters, mean coherence path dimensions, agreement factors for the Rietveld refinements, and specific surface areas of pure and Cr-substituted goethites.

Sample	G_0-60 h	G_0-20	G_5-20	G_7-20	G_7A-20	$G_{11.2}$-145	α-CrOOH
μ_{Cr} [mol mol^{-1}] (nominal)	0	0	6.2 ± 0.2	10.0 ± 0.2	37.5 ± 0.2	26.5 ± 0.2	–
μ_{Cr} [mol mol^{-1}] (ICPS)	0	0	5.0 ± 0.2	7.0 ± 02	7.0 ± 0.2	11.2 ± 0.2	–
Particle width and length [nm]	1980–102	850–85	620–110	590–116	–	850–230	–
a [Å]	4.6092(2)	4.6134(2)	4.6117(2)	4.6057(1)	–	4.5965(2)	4.492(3)
b [Å]	9.9582(2)	9.9601(2)	9.9580(2)	9.9551(2)	–	9.9516(2)	9.860(5)
c [Å]	3.0237(1)	3.0243(1)	3.0217(1)	3.0203(1)	–	3.0172(1)	2.974(2)
Volume [$Å^3$]	138.787(8)	138.967(10)	138.737(4)	138.481(11)	–	138.017(8)	131.722(24)
L_{paral} [nm]	41	42	40	40	–	49	–
L_{perp} [nm]	139	185	312	513	–	786	–
wRp	5.74	9.67	8.40	11.37	–	8.68	–
Rp	4.81	7.69	6.85	8.14	–	7.06	–
Chi^2	1.22	1.30	1.46	1.46	–	1.80	–
R_{Bragg}	3.78	4.55	4.14	4.60	–	4.85	–
SSA [m^2gr^{-1}]	38.81 ± 3.29	36.06 ± 3.06	14.72 ± 1.25	18.52 ± 1.57	–	23.92 ± 2.03	–

Notes:
$Rp = 100\Sigma|Io - Ic|/\Sigma Io$; $wRp = 100[\Sigma wi(Io - Ic)^2/\Sigma(wiIo)^2]^{0.5}$; $R_{Bragg} = 100\Sigma|Iko - Ikc|/\Sigma Iko$; $Chi^2 = \Sigma wi(Io - Ic)^2/(N - P)$. *Io* and *Ic* = observed and calculated intensities. wi = weight assigned to each step intensity. Iko and Ikc = observed and calculated intensities for Bragg k-reflection. N and P = number of data points in the pattern and number of parameters refined. Values in parentheses are esd for the least significant figures of the data shown, the esd values are taken from the final cycle of the Rietveld refinement.

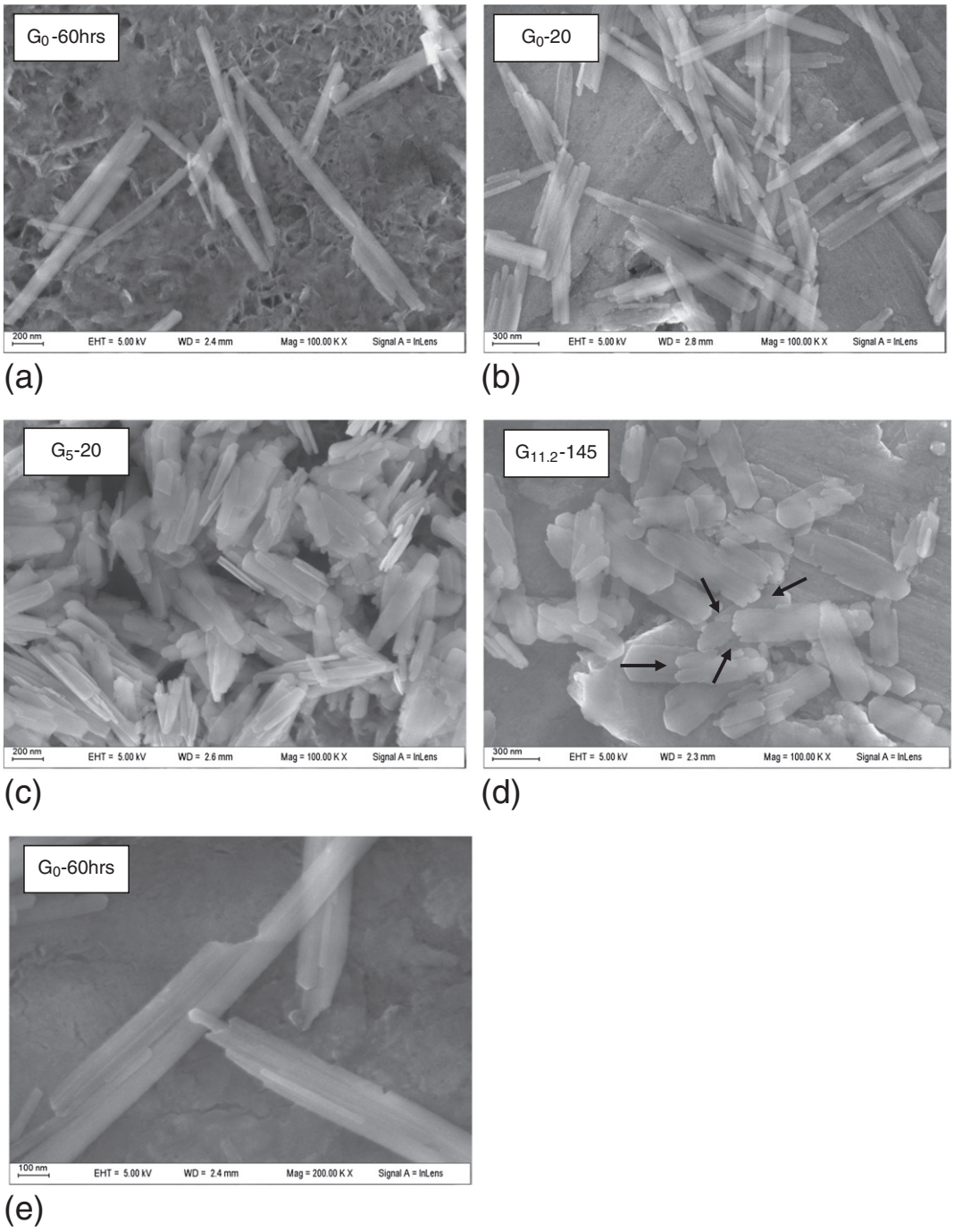

Fig. 1. SEM micrographs of selected samples, magnification 100,000×: (a) G_0-60 h, av. size 1980×102 nm; (b) G_0-20, av. size 850×85 nm; (c) G_5-20, av. size 620×110 nm; (d) $G_{11.2}$-145, av. size 850×230 nm; (e) G_0-60 h, magnification 200,000×. Average sizes obtained by measuring about 90 particles of each sample. Arrows show surface etching.

refinements is similar for all samples, and the reliability factors in the range: wRp = 5.74–11.37; Rp = 4.81–8.14 and R_B = 3.78–4.85, and χ^2 values between 1.22 and 1.86, are adequate.

All samples present different lattice parameters and crystallite (or MCP) sizes. Pure goethite prepared using 1 M KOH, displays a smaller cell volume than the one prepared using 3 M KOH. The cell parameters of the Cr-incorporated samples decreased with Cr content, showing cell values that tend to those of bracewellite. This decrease was taken as evidence for Cr-for-Fe substitution (Schwertmann et al., 1989; Sileo et al., 2004). No other peaks corresponding to pure bracewellite were detected, indicating than pure α-CrOOH was not formed, and that the Cr ions are incorporated in the goethite structure.

The calculated MCP dimensions shown in Table 1, and obtained from the Rietveld refinements of XRD data, reflect the domain or crystallite size parallel (L_{paral}), and perpendicular (L_{perp}) to the anisotropic broadening (110) axis, normal to (110) crystal plane. All MCP values in Table 1 are smaller than the particles dimensions shown in Fig. 1 and indicate the domainic character of the synthesized laths. The L_{paral} values, in the range 40 to 49 nm, do not change much in the series, but L_{perp}.values increased from 139 to 786 nm with Cr-content and aging time, indicating increasingly elongated domains. The average L_{paral} value is very close to the height of the parallel sub-units shown in Fig. 1-(b).

The variations in the average width and length values of the particles, and the increment of the calculated MCP dimensions indicated

that the number of crystalline domains per particle is lower in the samples aged for a longer period and in samples with higher μCr values ($G_{11.2}$-145). These results confirm that lattice parameters and crystallinity depend not only on the Cr-for-Fe substitution but also on the preparative pH conditions and the time of aging.

The specific surface areas (SSA), measured using the BET method, are presented in Table 1 for all samples. Sample G_0-60 h, with the largest particle size, and smallest domains had the largest SSA value (38.81 m^2g^{-1}). Also, and accordingly with the calculated MCP dimensions, all Cr-goethites with increasing crystallinity showed lower area values than pure goethites. In the α-Cr,FeOOH series SSA increases with increased Cr-incorporation. This unexpected fact may be attributed to the surface etching observed in Fig. 1, and caused by the amorphous extraction process on the Cr-goethites. As the etching increases with the Cr-content, the observed trend in SSA values shows the interplay of increasing crystallinity (leading to smaller BET surface area), and increasing surface damage (leading to higher BET surface area).

3.4. Kinetic dissolution measurements

3.4.1. Reactivity in several acid media

Fig. 2 shows the fractions of Fe dissolved, f_{Fe} (f_{Fe} = dissolved Fe mass/total Fe mass) at 70 °C, plotted as function of reaction time for sample G_0-20 dissolved at pH 3.5 in 0.10 M H_2Oxal and 0.10 M $H_2Oxal/5.12\times10^{-4}$ M Fe(II), and in 3.98 M HCl. The kinetic runs show a deceleratory behavior.

The experimental data were fitted using three commonly used models: the contracting sphere model (three-dimensional geometry), the contracting cylinder model (bidimensional geometry), and the Kabai equation (Kabai, 1973). In a good agreement with SEM measurements that revealed an elongated form of the goethites particles, the bidimensional geometry model best described the kinetic behavior (i.e. yielded a straight line when a square root law was applied, see inset in Fig. 2). Within this model (Brown et al., 1980), the rate law expression, based on the assumption of isotropic dissolution, where the reaction proceeds inwards at a constant rate at all crystal surfaces, takes the following expression,

$$1-(1-f)^{1/2} = kt \quad (1)$$

where *k*, the dissolution rate constant expressed in s^{-1}, represents the advance of the reaction on the surface of the particle. The

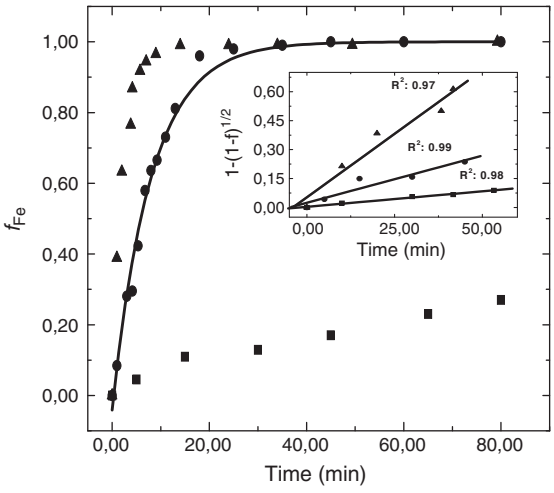

Fig. 2. Dissolution-time curves for G_0-20 in 0.1 M H_2Oxal, pH 3.5 (■); 3.98 M HCl (●) and 0.1 M H_2Oxal/Fe(II) 5.12×10^{-4}M, pH 3.5 (▲) at 70.00 °C. The solid line shows the deceleratory behavior. The application of the bidimensional contracting model for all data is shown in the inset; where the time values for (▲) and (●) were multiplied by a factor of 10 for comparative purposes.

Table 2
Experimental conditions and k values for the different dissolution measurements.

Sample	[HCl] [mol dm^{-3}]	[H_2Oxal] [mol dm^{-3}]	[Fe(II)] [mol dm^{-3}]	T [°C]	k [mol Fe s^{-1} m^{-2}]
G_0-60 h	0	0.1	5.12×10^{-4}	70	1.07×10^{-6}
G_0-60 h	0	0.1	5.12×10^{-4}	60	6.52×10^{-7}
G_0-60 h	0	0.1	5.12×10^{-4}	50	3.94×10^{-7}
G_0-60 h	0	0.1	5.12×10^{-4}	20	6.86×10^{-8}[a]
G_0-20	0.10	0	0	70	$<1.0\times10^{-11}$
G_0-20	3.98	0	0	70	1.67×10^{-7}
G_0-20	3.98	0	0	40	2.09×10^{-8}
G_0-20	0	0.10	0	70	7.16×10^{-9}
G_0-20	0	0.10	5.12×10^{-4}	70	9.88×10^{-7}
G_0-20	0	0.10	5.12×10^{-4}	60	6.58×10^{-7}
G_0-20	0	0.10	5.12×10^{-4}	50	3.77×10^{-7}
G_0-20	0	0.10	5.12×10^{-4}	20	6.94×10^{-8}[a]
G_5-20	3.98	0	0	70	9.14×10^{-9}
G_5-20	0	0.10	5.12×10^{-4}	70	8.03×10^{-7}
G_5-20	0	0.10	5.12×10^{-4}	60	4.10×10^{-7}
G_5-20	0	0.10	5.12×10^{-4}	50	2.87×10^{-7}
G_5-20	0	0.10	5.12×10^{-4}	20	4.73×10^{-8}[a]
G_7-20	0	0.10	7.11×10^{-5}	70	1.14×10^{-7}
G_7-20	0	0.10	1.32×10^{-4}	70	2.17×10^{-7}
G_7-20	0	0.10	2.74×10^{-4}	70	3.60×10^{-7}
G_7-20	0	0.10	6.35×10^{-4}	70	4.50×10^{-7}
G_7-20	0	0.10	5.12×10^{-4}	70	5.42×10^{-7}
G_7-20	0	0.10	8.92×10^{-4}	70	4.92×10^{-7}
G_7-20	0	0.10	7.66×10^{-4}	70	5.11×10^{-7}
G_7-20	0	0.10	5.12×10^{-4}	60	2.54×10^{-7}
G_7-20	0	0.10	5.12×10^{-4}	50	1.67×10^{-7}
G_7-20	0	0.10	5.12×10^{-4}	20	14.00×10^{-8}[a]
$G_{11.2}$-145	0	0.10	2.57×10^{-4}	70	5.12×10^{-8}
$G_{11.2}$-145	0	0.10	3.82×10^{-4}	70	9.77×10^{-8}
$G_{11.2}$-145	0	0.10	5.12×10^{-4}	70	1.03×10^{-7}
$G_{11.2}$-145	0	0.10	6.37×10^{-4}	70	1.30×10^{-7}
$G_{11.2}$-145	0	0.10	7.67×10^{-4}	70	1.45×10^{-7}
$G_{11.2}$-145	0	0.10	8.99×10^{-4}	70	1.45×10^{-7}
$G_{11.2}$-145	0	0.10	5.12×10^{-4}	50	2.74×10^{-8}
$G_{11.2}$-145	0	0.10	5.12×10^{-4}	40	7.72×10^{-9}
$G_{11.2}$-145	0	0.10	5.12×10^{-4}	20	1.54×10^{-9}[a]

[a] Calculated k values.

calculated dissolution constants k, expressed in mol Fe s^{-1} m^{-2} are shown for all samples in Table 2.

In order to compare the dissolving properties of HCl and H_2Oxal acids, some samples were dissolved in 0.10 M HCl, and in 0.10 M H_2Oxal, pH 3.5, at 70 °C. In contrast, with the behavior observed in 0.10 M HCl (dissolved Fe was detected only after 46 h), when oxalic acid was used, the solid dissolved in less than 2 h providing a k value of 7.16×10^{-9} mol Fe s^{-1} m^{-2}. The results indicated a higher reactivity in the complexing media, following the same behavior formerly found for other iron oxides (dos Santos Afonso et al., 1990; Figueroa et al., 2000). The increase in reactivity, when H_2Oxal was used, can be interpreted in terms of the surface complexation model (Blesa et al., 1994; Stumm and Morgan, 1995), based on the initial adsorption of the $HOxal^-$ ion onto the suspended oxide particles,

$$\equiv Fe(III)-OH + HOxal^- + H^+ \rightarrow \equiv Fe(III)-HOxal + H_2O, \quad (2)$$

$$\equiv Fe(III)-HOxal + 2\,Oxal^{2-} \rightarrow \equiv + [Fe(III)(Oxal)_3]^{3-}_{(aq)} + H^+, \quad (3)$$

whereas ≡ denotes the surface of the solid

The dissolution rate constant values, in the range 1.10^{-11}–$1.67.10^{-7}$ mol Fe s^{-1} m^{-2}, presented in Table 2 support the idea of the stability of these goethites in acid and complexing media. The very low reactivity shown by G_0-20 in 0.10 M HCl, demonstrates the known chemical inertia of goethite towards mineral acid dissolution.

The influence of the addition of Fe(II) to the complexing media was tested and k values increased (c.f. Table 2). For example, in sample G_0-20, the k value changed from 7.16×10^{-9} to 9.88×10^{-7} mol

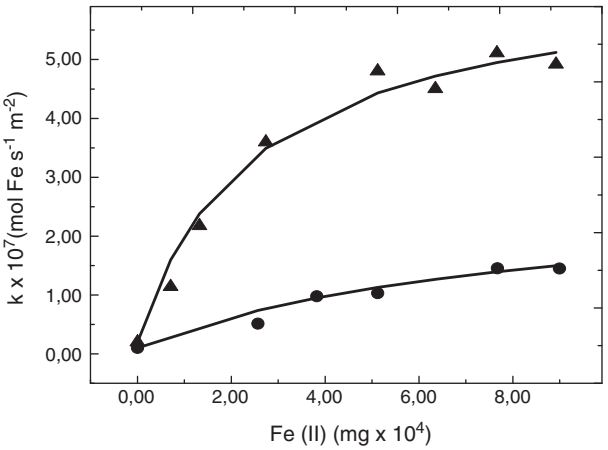

Fig. 3. Rate constant values for the dissolution of samples G_7-20 (▲) and $G_{11.2}$-145 (●) at 70 °C in 0.1 M oxalic acid, pH 3.5 as a function of $[Fe^{2+}]$. The points represent experimental data and the solid lines were calculated according to Eq. (7).

Fe s^{-1} m^{-2} when 5.12×10^{-4} M Fe(II) was added to the dissolving agent, at 70 °C. In presence of ferrous ion the following well-known reductive mechanism operates (Blesa et al., 2000; Stumm and Morgan, 1995),

$$\equiv Fe(III)-OH + [Fe(II)-(Oxal)_3]^{4-} + H^+ \rightarrow \equiv Fe(III)\bullet\bullet\bullet Oxal-Fe(II)-(Oxal)_2 + H_2O \quad (4)$$

$$\equiv Fe(III)\bullet\bullet\bullet Oxal-Fe(II)-(Oxal)_2 \rightarrow \equiv Fe(II)\bullet\bullet\bullet Oxal-Fe(III)-(Oxal)_2 \quad (5)$$

$$\equiv Fe(II)\bullet\bullet\bullet Oxal-Fe(III)-(Oxal)_2 + 3\,Oxal^{2-} \rightarrow \equiv + Fe(II)-(Oxal)_3^{4-} + Fe(III)-(Oxal)_3^{3-} \quad (6)$$

The charges of the surface complexes are omitted for simplicity.

In the presence of Fe(II), the rate constant of pure goethites practically remains unaltered in going from G_0-60 h to G_0-20, indicating that aging time does not play a significant role in the dissolution process. In the substituted samples, the k value at 70 °C decreased with Cr-content from 8.03×10^{-7} to 1.03×10^{-7} mol Fe s^{-1} m^{-2}. These low k values indicate the stabilizing effect of Cr against dissolution, even in a reductive media.

Data on Table 2 also indicated that the dissolution rates of sample G_0-20 in different acids and similar conditions ([acid] = 0.10 M, 70 °C), follow the trend HCl < H_2Oxal ≪ H_2Oxal/Fe(II). Although the dissolution behavior of the other samples in HCl 0.10 M and/or in 0.10 M H_2Oxal, pH 3.5, was not explored in this work, the same trend in dissolution can be extrapolated for the samples with greater Cr-content, because it is known that iron oxides present a higher reactivity than Cr-oxides (Blesa et al., 1994; Cotton and Wilkinson, 1988), and that the reactivity of mixed oxides is intermediate between the end members of the series (García Rodenas et al., 2008). The great increment of dissolution rate in H_2Oxal/Fe(II) must be taken into account when complexing acids (ex. humic acids) and Fe(II) are present in soils, greatly enhancing goethites dissolution.

3.4.2. Influence of the Fe(II) concentration on the dissolution

Fig. 3 shows the k values obtained for the dissolution of samples G_7-20 and $G_{11.2}$-145 at 70 °C in 0.10 M oxalic acid, pH 3.5, as a function of $[Fe^{2+}]$. At low adsorbate concentrations, both samples display a decelerating increase in k with ferrous ion concentration; a saturation effect is observed at the highest concentration of Fe(II). The observed dependence between k and $[Fe^{2+}]$ may be modeled using the following Langmuir modified equation:

$$k = k_0 + \frac{k_{max}\,K[Fe(II)]}{(1 + K[Fe(II)])} \quad (7)$$

where k_0 is related to the value of k in the absence of Fe(II), k_{max} is related to the maximum amount of Fe(II) that can be adsorbed to provide a monolayer coverage on the oxide particle, and K is a measure of the affinity of the adsorbate (Fe(II)) for the adsorbent (goethite particle). The calculated k_0, k_{max} and K values for samples G_7-20 and $G_{11.2}$-145 are shown in Table 3.

Values of k_0, k_{max} and K are lower in $G_{11.2}$-145 compared to G_7-20, and the calculated parameters point to the lesser reactivity of the sample with higher μ_{Cr} value. The decrease may be attributed to a lower concentration of surface complexes of the type, ≡Fe(III) ••• Oxal–Fe(II)–$(Oxal)_2$ (see Eq. (4)), because of the lower Fe/Cr ratio of sample $G_{11.2}$-145 when compared to G_7-20.

3.4.3. Congruency of dissolution

The release of Cr was also measured in the substituted goethites. The general form of Fe and Cr release, encountered in all samples, is shown in Fig. 4 for sample $G_{11.2}$-145. The constant ratio between f_{Fe}/f_{Cr} indicates identical (congruent) dissolution rates for Fe and Cr. This congruency provides information regarding the distribution of Cr within the particles (Singh and Gilkes, 1992; Wells, 1998), and the single straight line obtained indicates that Cr(III) is evenly distributed in the solid being dissolved. Although it is known that Cr(III) and Fe(III) oxides present different reactivity towards acid dissolution, the simultaneous leaching of both ions may be attributable to the disruption of the crystal network brought about by the Fe(III) dissolution that disrupts the structural framework, and labializes the Cr(III)–O bonds, facilitating the Cr(III) transfer to the solution. Similar results were reported by Sileo et al. (2006) and García Rodenas et al. (2008) for several substituted ferrites.

3.4.4. Relation between dissolution temperature and activation energy

The calculated activation energies (Ea) for the dissolution process of the samples using the Arrhenius equation ($k = A\,e^{-Ea/RT}$), are presented in Table 3. These values allowed us calculate the k values at 20 °C, presented in Table 2. The magnitude of Ea contains information on the reaction mechanism, and previous works (Laidler, 1964; Pilling and Seakins, 1995; Spiro, 1989; Su and Puls, 1999) have indicated that diffusion-controlled reactions present Ea values lower than 21 kJ mol^{-1}. The values in Table 3, in the range of 45.92 to 70.22 kJ mol^{-1}, rule out a diffusion control of the dissolution process and confirm the surface reaction control of the dissolution regime.

Table 3
Dissolution constants k_0, k_{max} and K for samples G_7-20 and $G_{11.2}$-145, and calculated Ea values for pure and Cr-substituted goethites.

Sample	G_0-60 h	G_0-20	G_5-20	G_7-20	$G_{11.2}$-145
k_0 (mol Fe s^{-1} m^{-2})	–	–	–	2.00×10^{-8}	1.00×10^{-8}
k_{max} (mol Fe s^{-1} m^{-2})	–	–	–	6.30×10^{-7}	2.70×10^{-7}
K	–	–	–	4000	1200
Ea (kJ mol^{-1})	45.92 (R^2: 0.99)	44.38 (R^2: 0.99)	47.32 (R^2: 0.99)	54.15 (R^2: 0.97)	70.22 (R^2: 0.96)

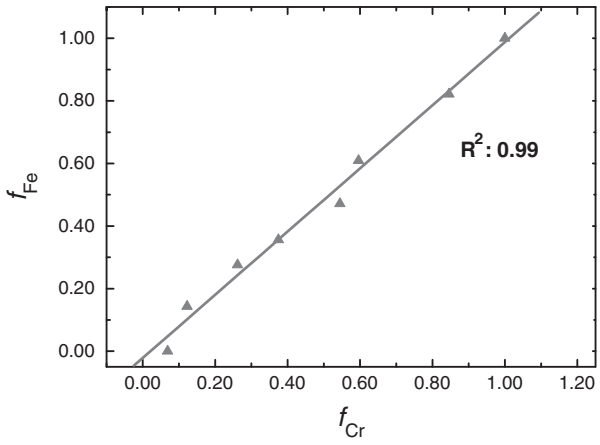

Fig. 4. Ratio between f_{Fe} vs f_{Cr} for the dissolution of $G_{11.2}$-145 at 70 °C in 0.1 M H_2Oxal/5.12×10^{-4} M Fe(II), pH 3.5.

The Ea values for the pure goethites samples G_0-60 h and G_0-20 (45.92 and 44.38 kJ mol^{-1}, respectively) do not differ much and may be considered equals within experimental error. However, the similar values point to the independence of Ea with aging time. This fact allows us to analyze the Ea values in the substituted goethites only as a function of Cr-incorporation, and to include sample $G_{11.2}$-145 in the same analysis. Table 3 shows that Ea increased with Cr-content indicating that the formation of the activated complex is inhibited in the presence of a surface that contains a higher Cr(III) concentration.

As the transformation of Cr-goethite to Cr-hematite is initiated around 250 °C (Sileo et al., 2004) the fate of Cr in these environments is intimately related to the dissolution process of Cr-hematites. Thus, we are currently conducting a similar study of substituted α-Fe_2O_3 and the preliminary results show some differences in the behavior of both oxides.

3.4.5. Influence of the aging time, crystallinity and Cr-content

As seen before the pH of the alkaline media used to prepare goethite greatly influences the morphology of the samples and larger particles were obtained at lower KOH concentrations. However, sample G_0-60 h, with the longest particle size (1980 × 102 nm), and higher number of domains per particle presents a higher k value than sample G_0-20 (MCP: 42 × 185 nm). Since k values are expressed per unit area, these results indicate that dissolution is more affected by the degree of domainicity, than by the particle size.

Data in Table 2 reveals that Cr-substitution decreases the dissolution constants of the substituted goethites. This result is in good agreement with those obtained by García Rodenas et al. (2008) for the dissolution of ferrites MFe_2O_4. These authors found that the dissolution rate is intermediate between those for the ferrite-forming oxides (Fe_2O_3 and MeO) and its determining step is a function of the surface concentration of the more reactive cation. In our case, this species is ≡Fe(III), whose concentration decreased with increasing Cr in the sample and supports the decrease in dissolution rate.

This indicates that in substituted goethites, with μ_{Cr} values in the range 5.0 to 11.2 mol%, the capacity for Cr-immobilization increased with Cr-content. The k values also indicate that, at 20 °C in a reductive and complexing media, pure goethite dissolves about 7 and 76 times faster than goethites with a Cr-content of 7.0 and 11.2 mol%.

4. Conclusions

Cr-incorporation in goethite increased with contact time, or aging, in the Cr-containing parent solution. The maximum Cr-incorporation in samples aged for 20 days was 7.0 mol%, and in samples aged for 145 days was 11.2 mol%.

The Cr-substitution modified the aspect of the particles, and increasing Cr-substitution produced wider particles. The Cr-content also modifies the MCP, or domain sizes, that are elongated and grow parallel to plane (110). The size of the domains was larger in the more substituted samples.

The particle size and cell dimensions of pure goethite varied with the preparation pH and larger sizes were obtained at lower KOH concentrations. XRD data confirmed that unit cell dimensions and crystallinity depend not only on the Cr-for-Fe substitution but also on the pH preparative conditions and on the aging history of the samples.

Goethite presented a good capacity for the immobilization of Cr-incorporated ions. The low k constant values presented in this work support the idea of the stability of pure and Cr-goethites in mineral acid and complexing media. The release of Fe and Cr decreased with Cr-substitution and highly substituted goethites retained Cr more efficiently than α-Cr,FeOOH with low levels of Cr.

The dissolution rate increased in the presence of oxalic acid and Fe(II) which affects the mobilization of Fe(III) and Cr(III), although the rate constant values were still low. The dissolution rate is largely determined by the degree of domainicity of the sample and, in similar acid concentration, dissolution follows the trend $HCl < H_2Oxal \ll H_2Oxal/Fe(II)$.

The effectiveness in Cr incorporation and the detected inertia towards dissolution indicated that Cr-contamination could be naturally attenuated by formation of goethite in aquifers as only 1 g of Cr-goethite may contain 6.5 mg of chromium. However, the complete dissolution of 6.5 mg Cr is sufficient to elevate the Cr-concentration of 6.5×10^3 L of natural water over the limits permitted by the ambient water quality criterion for the protection of human health (10 μg L^{-1}) adopted by the W.A. EPA (1993).

In order to generalize these remediation or attenuation mechanisms we are currently studying the retention capacity of several Fe iron oxides (v.g. hematite, akaganeite, magnetite). Also the applicability of these iron oxides for other metal remediation purposes is currently being explored.

Acknowledgments

This research was partially supported by grant from UBACYT X800 and PICT 0780 (2008). We thank Prof. M.A. Blesa for critical reading and useful suggestions.

References

Alvarez, M., Rueda, E.H., Sileo, E.E., 2006. Structural characterization and chemical reactivity of synthetic Mn-goethites and hematites. Chemical Geology 231, 288–299.
Alvarez, M., Rueda, E.H., Sileo, E.E., 2007. Simultaneous incorporation of Mn and Al in the goethite structure. Geochimica et Cosmochimica Acta 71, 1009–1020.
Alvarez, M., Sileo, E.E., Rueda, E.H., 2008. Structure and reactivity of synthetic Co-substituted goethites. American Mineralogist 93, 584–590.
Baes, C.F., Mesmer, R.E., 1976. The Hydrolysis of Cations. Wiley.
Banks, M.K., Schwab, A.P., Henderson, C., 2006. Leaching and reduction of chromium in soil as affected by soil organic content and plants. Chemosphere 62, 255–264.
Baumgartner, E., Blesa, M.A., Maroto, A.J.G., 1982. Kinetics of the dissolution of magnetite in thioglycolic acid solutions. Journal of the Chemical Society Dalton Transactions 1649–1654.
Baumgartner, E., Blesa, M.A., Marinovich, H., Maroto, A.J.G., 1983. Heterogeneous electron transfer as a pathway in the dissolution of magnetite in oxalic acid solutions. Inorganic Chemistry 22, 2224–2226.
Blesa, M.A., Marinovich, H.A., Baumgartner, E.C., Maroto, A.J.G., 1987. Mechanism of dissolution of magnetite by oxalic acid-ferrous ion solutions. Inorganic Chemistry 26, 3713–3717.
Blesa, M.A., Morando, P.J., Regazzoni, A.E., 1994. Chemical Dissolution of Metal Oxides. CRC Press. Inc, Boca Raton, Fla., USA.
Blesa, M.A., Weisz, A.D., Morando, P.J., Salfity, J.A., Magaz, G.E., Regazzoni, A.E., 2000. The interaction of metal oxide surfaces with complexing agents dissolved in water. Coordination Chemistry Reviews 196, 31–63.
Borghi, E.B., Regazzoni, A.E., Maroto, A.J.G., Blesa, M.A., 1989. Reductive dissolution of magnetite by solutions containing EDTA and Fe^{II}. Journal of Colloid and Interface Science 130, 299–310.

Brown, W.E., Dollimore, D., Galwey, A., 1980. In: Bamford, C.H., Tipper, C.F.H. (Eds.), Reactions in the Solid State, Comprehensive Chemical Kinetics, vol. 22. Elsevier, Amsterdam.
Carvalho-e-Silva, M.L., Ramos, A.Y., Tolentino, H.C.N., Enzweiler, J., Netto, S.M., Martins Alves, M.C., 2003. Incorporation of Ni into natural goethite: an investigation by X-ray absorption spectroscopy. American Mineralogist 88, 876–882.
Cornell, R.M., Schwertmann, U., 1996. The Iron Oxides: Structure, Properties, Reactions, Occurrence and Uses. VCH, Weinheim, Federal Republic of Germany.
Cotton, F.A., Wilkinson, G., 1988. Advanced Inorganic Chemistry, 5ª ed. Wiley, New York, USA.
Cummings, D.A., March, A.W., Bostick, B., Spring, S., Caccavo Jr., F., Fendorf, S., Frank, Rosenzweig R., 2000. Evidence for microbial Fe(III) reduction in anoxic, mining-impacted lake sediments (Lake Coeur d'Alene, Idaho). Applied and Environment Microbiology 66, 154–162.
dos Santos Afonso, M., Morando, P.J., Blesa, M.A., Banwart, S., Stumm, W., 1990. The reductive dissolution of iron oxides by ascorbate. Journal of Colloid and Interface Science 138, 74–82.
Figueroa, C.A., Sileo, E.E., Morando, P.J., Blesa, M.A., 2000. Dissolution of nickel ferrites in aqueous solutions containing oxalic acid and ferrous salts. Journal of Colloid and Interface Science 225, 403–410.
García Rodenas, L.A., Blesa, M.A., Morando, P.J., 2008. Reactivity of metal oxides: thermal and photochemical dissolution of MO and MFe_2O_4 (M Ni, Co, Zn). Journal of Solid State Chemistry 181, 2350–2358.
Gasser, U.G., Nuesch, R., Singer, M.J., Jeanroy, E., 1999. Distribution of manganese in synthetic goethite. Clay Minerals 34, 291–299.
Gerth, J., 1990. Unit-cell dimensions of pure and trace metal-associated goethites. Geochimica et Cosmochimica Acta 54, 363–371.
Hingston, J.A., Collins, C.D., Murphy, R.J., Lester, J.N., 2001. Leaching of chromated copper arsenate wood preservatives: a review. Environmental Pollution 111, 53–56.
Kabai, J., 1973. Determination of specific activation energies of metal oxides and metal oxide hydrates by measurement of the rate of dissolution. Acta Chimica Academiae Scientiarum Hungaricae 78, 57–73.
Kaur, N., Singh, B., Kennedy, B.J., Gräfe, M., 2009a. The preparation and characterization of vanadium substituted goethite: the importance of temperature. Geochimica et Cosmochimica Acta 73, 582–593.
Kaur, N., Gräfe, M., Singh, B., Kennedy, B.J., 2009b. Simultaneous incorporation of Cr, Zn, Cd and Pb in the goethite structure. Clays and Clay Minerals 57, 234–250.
Kaur, N., Singh, B., Kennedy, B.J., 2009c. Copper substitution alone and in the presence of chromium, zinc, cadmium and lead in goethite (α-FeOOH). Clay Minerals 44, 293–310.
Kaur, N., Singh, B., Kennedy, B.J., 2010. Dissolution of Cr, Cd, Zn and Pb single- and multi-metal substituted goethite; relation to structural, morphological, and dehydroxylation properties. Clays and Clay Minerals 58, 415–430.
Khan, B.I., Solo-Gabriele, H.M., Townsend, T.G., Cai, Y., 2006. Release of arsenic to the environment from CCA-treated wood. 1. Leaching and speciation during service. Environmental Science and Technology 40, 988–993.
Laidler, K.J., 1964. Chemical Kinetics. McGraw-Hill, New York.
Larson, A.C., Von Dreele, R.B., 1994. General structure analysis system (GSAS, Los Alamos National Laboratory Report LAUR 86–748.
Leussing, D.L., Newman, L., 1956. Spectrophotometric study of the bleaching of ferric thioglycolate. spectrophotometric study of the bleaching of ferric thioglycolate. Journal of the American Chemical Society 78, 552–556.
Lewis, D.G., Schwertmann, U., 1979. The influence of Al on iron oxides. Part III. Preparation of Al goethites in 1 M KOH. Clay Minerals 23, 115–126.
Lim-Nunez, R., Gilkes, R.J., 1987. Acid dissolution of synthetic metal-containing goethite and hematites. Proceedings of the International Clay Conference, Clay Minerals Society of America, Denver, pp. 197–204.
Lovley, D.R., Holmes, D.E., Nevin, K.P., 2004. Dissimilatory Fe(III) and Mn(IV) reduction. Advances in Microbial Physiology, vol. 49. Elsevier, Amsterdam, pp. 219–286.
Manceau, A., Schlegel, M.L., Musso, M., Sole, V.A., Gauthier, C., Petit, P.E., Trolard, F., 1999. Crystal chemistry of trace elements in natural and synthetic goethite. Geochimica et Cosmochimica Acta 64, 3643–3661.
Milton, C., Appleman, D.E., Appleman, M.H., Chao, E.C.T., Guttita, F., Dinnin, J.D., Dwornik, E.J., Ingram, B.L., Rose, H.J., 1976. Merumite, a complex assemblage of chromium minerals from Guyana. Geological Survey Professional Paper 887, 1–29.
Murad, E., Schwertmann, U., 1983. The influence of aluminum substitution and crystallinity on the Mössbauer spectra of goethite. Clay Minerals 18, 301–312.
Norrish, K., 1975. Geochemistry and mineralogy of trace elements. In: Nicholas, A.R., Egan, D.J. (Eds.), Trace Elements in Soil–Plant–Animal System. Academic Press, New York, pp. 55–81.
Persson, P., Axe, K., 2005. Adsorption of oxalate and malonate at the water–goethite interface: molecular surface speciation from IR spectroscopy. Geochimica et Cosmochimica Acta 69, 541–552.
Pilling, M.J., Seakins, P.W., 1995. Reaction Kinetics. Oxford University Press, New York.
Pozas, R., Rojas, C.T., Ocana, M., Serna, C.J., 2004. The nature of Co in synthetic Co-substituted goethites. Clays and Clay Minerals 52, 760–766.
Rasem Hasan, A., Hub, L., Solo-Gabriele, H.M., Fieber, L., Cai, Y., Townsend, T.G., 2010. Field-scale leaching of arsenic, chromium and copper from weathered treated wood. Environmental Pollution 158, 1479–1486.
Ruan, H.D., Gilkes, R.J., 1995. Dehydroxylation of aluminous goethite: unit cell dimensions, crystal size and surface area. Clays and Clay Minerals 43, 196–211.
Schwertmann, U., 1984. The influence of aluminum on iron oxides. IX. Dissolution of Al-goethites in 6 M HCl. Clay Minerals 22, 83–92.
Schwertmann, U., Cornell, R.M., 2000. Iron Oxides in the Laboratory, Preparation and Characterization, 2nd edition. Wiley-VCH, Weinheim, Germany.
Schwertmann, U., Taylor, R.M., 1989. Iron oxides. In: Dixon, J.B., Weed, S.B. (Eds.), Minerals in Soil Environments. Soil Sci. Soc Am., Madison, WI, pp. 380–438.
Schwertmann, U., Gasser, U., Sticher, H., 1989. Chromium-for iron substitution in synthetic goethites. Geochimica et Cosmochimica Acta 53, 1293–1297.
Sileo, E.E., Alvarez, M., Rueda, E.H., 2001. Structural studies on the manganese for iron substitution in the synthetic goethite–jacobsite system. International Journal of Inorganic Materials 3, 271–279.
Sileo, E.E., Ramos, A.Y., Magaz, G., Blesa, M.A., 2004. Long-range vs. short-range ordering in synthetic Cr-substituted goethites. Geochimica et Cosmochimica Acta 68, 3053–3063.
Sileo, E.E., Garcia Rodenas, L., Paiva Santos, C.O., Stephens, P.W., Morando, P.J., Blesa, M.A., 2006. Correlation of reactivity with structural factors in a series of Fe(II) substituted cobalt ferrites. Journal of Solid State Chemistry 179, 2237–2244.
Singh, B., Gilkes, R.J., 1992. Properties and distribution of iron oxides and their association with minor elements in the soils of south-western Australia. Journal of Soil Science 43, 77–98.
Singh, B., Sherman, D.M., Gilkes, R.J., Wells, M., Mosselmans, J.F.W., 2002. Incorporation of Cr, Mn and Ni into goethite (α-FeOOH): Mechanism from extended X-ray absorption fine structure spectroscopy. Clay Minerals 37, 639–649.
Singh, B., Grafe, M., Kaur, N., Liese, A., 2010. Applications of Synchrotron-based X-ray diffraction and X-ray absorption spectroscopy to the understanding of poorly crystalline and metal-substituted iron oxides. Balwant Singh and Markus Gräfe: Developments in Soil Science, 34. Elsevier B.V., The Netherlands, pp. 199–254.
Skovbjerg, L.L., Stipp, S.L.S., Utsunomiya, S., Ewing, R.C., 2006. The mechanism of reduction of hexavalent chromium by green rust sodium sulphate: formation of Cr-goethite. Geochimica et Cosmochimica Acta 70, 3582–3592.
Sparks, D.L., 2003. Environmental Soil Chemistry, 2nd edition. Academic Press, San Diego, CA.
Spiro, M., 1989. In: Compton, R.G. (Ed.), Reactions at the Liquid–solid Interface, Chemical Kinetics, vol. 28. Elsevier, Amsterdam.
Stiers, W., Schwertmann, U., 1985. Evidence for manganese substitution in synthetic goethite. Geochimica et Cosmochimica Acta 49, 1909–1911.
Stone, A.T., 1986. Adsorption of organic reductants and subsequent electron transfer on metal oxide surfaces. In: Sparks, D.L., Suarez, D.L. (Eds.), Rates of Soil Chemical Processes. : SSSA Spec. Publ., 27. Soil Sci. Soc. Am., Madison, WI.
Stumm, W., Morgan, J.J., 1995. Aquatic Chemistry: Chemical Equilibria and Rates in Natural Waters, 3rd ed. Wiley-Interscience Pub., USA.
Su, C., Puls, R.W., 1999. Kinetics of Trichloroethene reduction by zerovalent iron and tin: pretreatment effect, apparent activation energy, and intermediate products. Environmental Science and Technology 33, 163–168.
Suter, D., Siffert, C., Sulzberger, B., Stumm, W., 1988. Catalytic dissolution of iron(III) (hydr)oxides by oxalic acid in the presence of Fe(II). Die Naturwissenschaften 75, 571–573.
Szytula, A., Burewicz, A., Dimitrijevic, Z., Krasnicki, S., Rzany, H., Todorovic, J., Wanic, A., Wolski, W., 1968. Neutron diffraction studies of α-FeOOH. Physica Status Solidi 26, 429–434.
Thompson, P., Cox, D.E., Hastings, J.B., 1987. Rietveld refinement of Debye–Scherrer synchrotron X-ray data from Al_2O_3. Journal of Applied Crystallography 20, 79–83.
Toby, B.H., 2001. EXPGUI, a graphical user interface for GSAS. Journal of Applied Crystallography 34, 210–213.
U.S. EPA, 1998. Toxicological Review of Hexavalent Chromium. U.S. Environmental Protection Agency, Washington, DC.
W.A. EPA, 1993. Western Australian Quality Guidelines for Fresh and Marine Water. EPA Bulletin N° 711. Western Australian Environmental Protection Authority, Perth.
Weber, K.A., Achenbach, L.A., Coates, J.D., 2006. Microorganisms pumping iron: anaerobic microbial iron oxidation and reduction. Nature Reviews Microbiology 4 (10), 752–764.
Wells, M.A., 1998. Mineral, chemical and magnetic properties of synthetic, metal substituted goethite and hematite. PhD Thesis. Faculty of Natural and Agricultural Sciences, University of Western Australia.
Wells, M.A., Fitzpatrick, R.W., Gilkes, R.J., 2006. Thermal and mineral properties of Al-, Cr-, Ni- and Ti-substituted goethite. Clays and Clay Minerals 54, 176–194.
Williams, A.G.B., Scherer, M.M., 2004. Spectroscopic evidence for Fe(II)–Fe(III) electron transfer at the iron oxide–water interface. Environmental Science and Technology 38, 4782–4790.